Synchronized delivery of Er:YAG-laser pulses into water studied by a laser beam transmission probe for enhanced endodontic treatment

P. Gregorčič[1] · N. Lukač[1] · J. Možina[1] · M. Jezeršek[1]

Abstract We examine the effects of the synchronized delivery of multiple Er:YAG-laser pulses during vapor-bubble oscillations into water. For this purpose, we used a laser beam transmission probe that enables monitoring of the bubble's dynamics from a single shot. To overcome the main drawbacks of this technique, we propose and develop an appropriate and robust calibration by simultaneous employment of shadow photography. By using the developed experimental method, we show that the resonance effect is obtained when the second laser pulse is delivered at the end or slightly after the first bubble's collapse. In this case, the resonance effect increases the mechanical energy of the secondary bubble's oscillations and prolongs their duration. The presented laser method for synchronized delivery of Er:YAG-laser pulses during bubble oscillations has great potential for further improvement of laser endodontic treatment, especially upon their safety and efficiency.

1 Introduction

Effective irrigation, including debriding, cleaning, and decontamination of anatomical cavities, is one of the most important challenges in different areas of dentistry, such as endodontics, implantology, periodontics, and bone surgery [1]. For example, one of the main goals in nonsurgical endodontic treatment is the efficient cleaning and decontamination of the smear layer, bacteria and dentine debris within the root canal system [2]. Recent studies [2, 3] have proven that the usage of a free-running erbium:yttrium aluminum garnet (Er:YAG) laser that radiates low-energy pulses (20–60 mJ) with durations of 50 μs is a very promising technique for endodontic treatment of the root canal. In these treatments, the Er:YAG-laser pulse with a wavelength of 2.94 μm is delivered through a fiber tip into the coronal portion of the pulpa chamber, filled with a liquid, such as water or sodium hypochlorite. Due to the very high absorption coefficient ($\mu_a = 1.247 \times 10^6$ m^{-1}) [4] of Er:YAG, light in water more than 70 % of all the pulse's light is absorbed within an only 1-μm-thick water layer. Thus, the water is locally and instantly heated over its boiling point, and a vapor bubble develops at the fiber tip's end [5–8].

Due to explosive boiling, the vapor bubble starts to expand. When it reaches its maximum volume, it is nearly empty and it collapses due to the pressure of the surrounding liquid. This collapse, in turn, initiates the secondary bubble's growth and collapse. The process repeats itself, resulting in the so-called secondary vapor-bubble's oscillations [9]. Here, each oscillation has less energy and therefore reaches smaller volume due to the energy dissipation during each oscillation [10–12]. The ratio between the mechanical energy of two successive oscillations was defined as the oscillation energy-conversion efficiency.

The main aim of this paper was to use a laser beam transmission probe (LBTP) [11, 13, 14] for examination of the synchronized delivery of multiple Er:YAG-laser pulses into water. Here, the first pulse induces a vapor bubble, while the role of the subsequent pulses is to increase the oscillation energy-conversion efficiency and to prolong the duration of acoustic transients. Therefore, we deliver the secondary pulse(s) during the bubble's oscillations. The presented method and results of synchronized delivery of

✉ P. Gregorčič
peter.gregorcic@fs.uni-lj.si

[1] Faculty of Mechanical Engineering, University of Ljubljana, Aškerčeva 6, 1000 Ljubljana, Slovenia

multiple Er:YAG pulses (called also photo acoustic synchronized transients; PHAST) are important since they have a great potential to open new opportunities for further development of modern, laser-based dental treatments and to further improve upon their safety and efficiency.

To examine the resonance effect of the oscillation energy-conversion efficiency as a function of the delay between the primary and the secondary Er:YAG pulse, we use a LBTP that *directly* measures the bubbles dynamics, and it is therefore able to detect the exact times of all the bubble's collapses and maximum volumes from a *single* shot. This inherent ability of the developed LBTP technique is especially important in modern endodontic treatments, where—instead of the amplitude—the duration of laser-induced destruction of bacteria should be prolonged. From this point of view, a synchronized delivery of Er:YAG pulses promises a great potential in new, still developing, medical approaches, where—due to prolonged times—the bacteria may be efficiently killed at lower amplitudes. Since higher amplitudes lead to higher collateral damage, this promises not only more efficient, but also safer treatment.

On the other hand, the LBTP only *indirectly* measures the bubbles volume that is important for the determination of the energy-conversion efficiency [8]. Therefore, an appropriate calibration method is needed for measuring the volume, independently on the bubble's shape. Due to this reason, the second important goal of this paper was to develop LBTP calibration by using laser shadowgraphy. Such a calibration deserves great interest in different experiments for investigations of laser-induced bubbles in liquids [8, 14–18], where LBTP can be used for online monitoring of bubble's dynamics.

2 Materials and methods

2.1 Experimental setup

Experimental setup is schematically presented in Fig. 1. As an excitation source, we used a free-running Er:YAG laser (Fotona, d.d., Slovenia, LightWalker) with a wavelength of 2.940 μm, designed for laser dentistry. The laser enables one or multiple pulses of full width at half maximum (FWHM) less than 1 μs and with peak powers between 1.5 and 2 kW (e.g., see the blue curves in Fig. 5). In the case of multiple pulses, the subsequent pulses are separated by an adjustable delay in the range between 10 μs and 1 ms.

To monitor the Er:YAG-pulse power as a function of time, we placed a 60-MHz InAs photodiode (PD-InAs) just behind the rear mirror of the laser resonator (LR). The signal from photodiode was acquired by a digital oscilloscope (LeCroy, US, 600 MHz Wave Runner 64MXi-A).
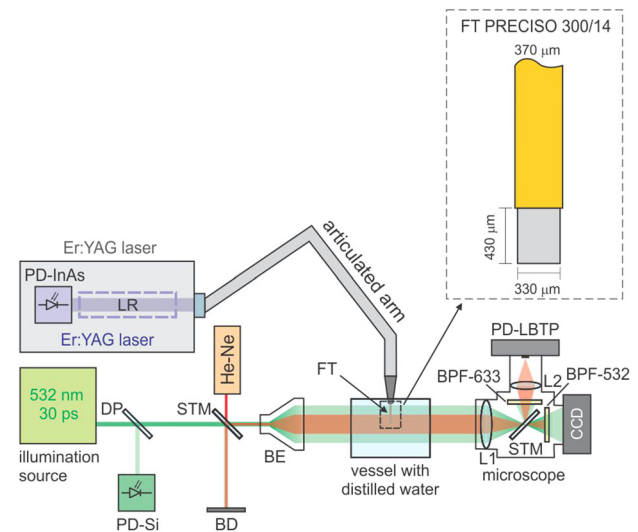

Fig. 1 Experimental setup including a free-running Er:YAG source, and two monitoring methods: a laser shadowgraphy (*green*, pulsed illumination) and a laser beam transmission probe (*red*, continuous-wave illumination)

The pre-calibration by using a power meter (Ophir Optronics Inc., Israel, Smart head to USB interface with a pyroelectric sensor PE50BF-DIF-SH-U2) was performed to convert the measured PD-InAs voltage into pulse power, as described in detail in Ref. [8].

The laser pulses were delivered into the vessel with distilled water through an articulated arm. Within the handpiece, the pulse was optically coupled into an interchangeable fiber tip (FT). In our experiments, we used the Fotona Preciso 300/14 fiber tip, schematically shown in the inset of Fig. 1. The FT was 14 mm long and had a flat end with a diameter of 300 μm.

The Er:YAG–pulse-water interaction induces a vapor bubble [6, 8]. We simultaneously monitored its dynamics by two measuring methods: laser shadow photography [8] and a LBTP [11]. The experimental setup was automatically controlled by using custom developed software, running on a personal computer. The used experimental software enables data acquisition from a digital oscilloscope, image acquisition, and also image and data processing.

2.1.1 Laser shadow photography

We employed laser-based shadow photography to observe the spatial distribution of vapor bubble in different time instances. The main idea of this technique is to use a short illumination pulse to "freeze" the motion of the fast phenomena. The shorter the illumination pulse is, the higher spatial resolution is achieved at given velocity of the observing phenomena. We used a frequency-doubled Nd:YAG laser (Ekspla, Lithuania, PL2250-SH-TH)

emitting green ($\lambda = 532$ nm) pulses with duration of 30 ps as an illumination source. The illumination pulse firstly passes a dielectric plate (DP) that reflects ~ 4 % of its light into the 1-GHz Si photodiode (PD-Si). The signal from PD-Si was used to determine the accurate time between the Er:YAG and the illumination-laser pulses. After DP, the illumination pulse passes the semi-transparent mirror (STM) enabling us to employ two measuring techniques, a shadowgraphy and LBTP, simultaneously in our experiment. To expand the illumination pulse over the whole Er:YAG–pulse-water interaction area, we used a beam expander (BE).

After BE, the light rays of the illumination pulse are parallel before reaching the vapor bubble. The rays that reach the bubble refracts due to the refractive-index gradients on its wall. This casts a shadow that can be visible on the screen [19]. Instead of the screen, we used a microscope equipped by a charge coupled device (CCD) camera (Basler AG, Germany, scA1400-17 fm, 1.4 Mpx). Here, the CCD camera is opened before the radiation of the illumination pulse and closes after the illumination pulse is already radiated. In such a way, the shadowgraph image of a single event is acquired. The excitation laser, illumination pulse, and camera were synchronized with a signal generator (Tektronix, US, AFG 3102).

Laser shadowgraphy enables two-dimensional spatial observations of laser-induced phenomena, but only in a single time instance [20]. Thus, multiple events (from multiple Er:YAG shots) should be captured at different time delays between the Er:YAG and illumination pulse to acquire the bubble's dynamics.

2.1.2 Laser beam transmission probe

To observe the whole dynamics from a single Er:YAG-laser shot, we simultaneously employed another measuring method, called a laser beam transmission probe (LBTP). The main idea of this technique is very similar to the idea of the shadow photography, since it also detects the refractive-index gradients. The main difference between the LBTP and the shadow photography is that LBTP is able to detect the whole bubble's dynamics from *a single* shot, but it cannot detect its 2D spatial distribution.

As an illumination source, LBTP uses a continuous-wave (CW) illumination probe. For this purpose, we employed a He–Ne laser. Its beam path is shown by the red line in Fig. 1. To couple the CW probe into the same path as the pulsed illumination for the shadowgraphy, we used a semi-transparent mirror (STM). The part of the beam not deflected by STM was damped by a beam dump (BD). After the coupling, the CW probe was led through the same BE as the pulsed illumination and it illuminates the same area as the illumination pulse for shadowgraphy.

Additional semi-transparent mirror (STM) was used inside the microscope (after the lens L1) to deflect the CW probe into the lens L2. Lens L2 collects all the transmitted CW-probe light into the 150-MHz Si photodiode (PD-LBTP). A narrow band-pass filter (BPF-633), centered at 633 ± 10 nm, was placed in front of L2 to block the green pulse used for the shadowgraphic method. And vice versa, another band-pass filter (BPF-532), centered at 532 ± 10 nm, was placed in front of CCD camera to block the light from He–Ne laser.

3 Results and discussion

3.1 Dynamics of bubble induced by a single pulse

Figure 2 shows a typical series of shadowgraphs for a single Er:YAG pulse with FWHM of 0.8 ± 0.2 μs and pulse energy of 2.0 ± 0.2 mJ (e.g., typical power as a function of time is shown by the blue curve in Fig. 3). Since the FT and the vapor bubble locally change the refractive index, they both appear as a dark area on the bright background due to the refraction of the pulsed probe on the refractive-index gradient.

In our previous work [8], we showed that a channel-like bubble is formed, when an Er:YAG pulse of duration longer than 40 μs is delivered into water through a 300-μm flat-end FT and that the spherical bubble forms for the conical FT. However, results, presented in Fig. 2, reveal that a spherical bubble develops also in case of the flat-end fiber tip, if a pulse with duration below 1 μs is used. This finding is in accordance with the results obtained by Jansen et al. [21], who compared the bubbles induced by a Ho:YAG laser in water.

Figure 3 shows a typical transmittance of the LBTP signal as a function of time. Since lens L2 (see Fig. 1) collects all of the CW-probe light on a single photodetector, the LBTP technique measures the transmittance $T(t)$ of the CW probe that can be calculated as the normalized LBTP signal:

$$T(t) = \frac{U(t)}{U_0}. \tag{1}$$

Here, $U(t)$ is the LBTP signal as a function of time, and U_0 is the LBTP signal before the Er:YAG pulse is delivered.

As visible from Fig. 3, at the beginning the transmittance is $T(t < 0) = 1$ and it starts to decrease with increasing bubble. When bubble reaches its maximum volume, the transmittance reaches its minimum value, as can be seen from the fourth orange square in Fig. 3 corresponding to the 4th image on Fig. 2a. At its maximum volume, the bubble is nearly empty and it, therefore, starts to collapse due to the pressure of the surrounding liquid.

Fig. 2 Typical series of shadowgraphs of a vapor bubble, induced by a single Er:YAG-laser pulse with FWHM of 0.8 ± 0.2 µs and pulse energy of 2.0 ± 0.2 mJ. **a** Bubble during its first oscillation. **b** The second and the third bubble's oscillations. The time after the Er:YAG pulse is shown on the *bottom-left-hand side* of each image
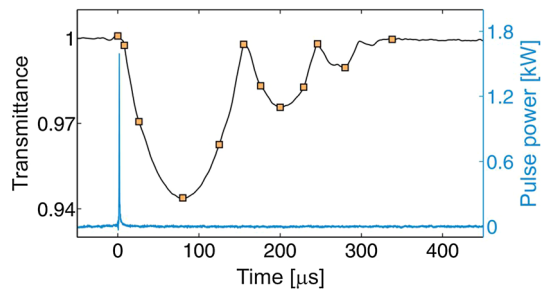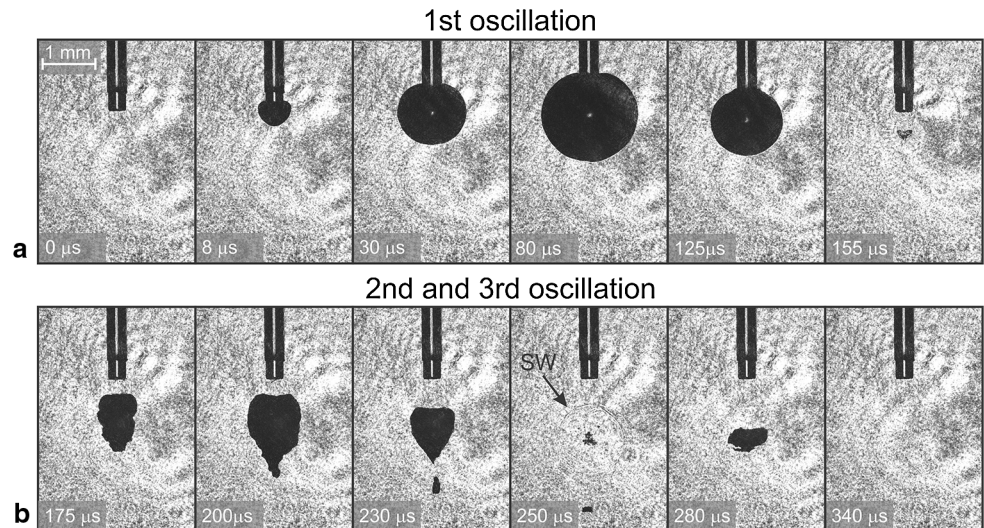

Fig. 3 Typical LBTP signal (the *left-hand-side axis* and the *red curve*) for a single Er:YAG-laser pulse (the *right-hand-side axis* and the *blue curve*). The *orange squares* show the events from Fig. 2

During the bubble's collapse, the LBTP transmittance increases. At the end of the collapse, the bubble almost disappears (e.g., see the last image of Fig. 2a) and the LBTP probe reaches values near 1 as is visible from the sixth square in Fig. 3. The process repeats several times, until the bubble's oscillations disappear due to the energy dissipation. Since the bubble is induced in an infinite liquid, a shock wave (denoted by SW in Fig. 2) is emitted at the end of each collapse. This is in accordance with the results, obtained by Gregorčič et al. [8].

3.2 Calibration of the laser beam transmission probe by shadow photography

LBTP has several drawbacks that should be improved by an appropriate calibration. The first drawback of this method is that the probe beam does not have a top hat profile. Instead, the intensity profile of the used probe beam is Gaussian. That means that if someone moves the bubble with constant volume within the CW probe, the signal will change due to non-uniform probe-intensity distribution. Another drawback of this method is that its response

significantly depends on the bubble's shape. To avoid the mentioned drawbacks, we performed the calibration by using shadow photography that has been simultaneously employed in our experiments.

The main idea of calibration is to measure the volume $V_B(t)$ of the bubble by shadow photography and the LBTP transmittance $T(t)$ at the same time t. Here, the bubble's volume is calculated by an image-processing algorithm, described in Ref. [8]. The used algorithm assumes that the vapor bubble is cylindrically symmetrical around the FT axis. In such a way, we measured the calibrating points $P_i = (T_i, V_{Bi})$. Due to different bubbles shapes and positions, each oscillation needs its own calibration. For the first, second, and third oscillations, induced by a single pulse (SP) and double pulse (DP), the calibrating points are shown by dots in Fig. 4. They are approximated by the polynomial of the second degree:

$$V_B = p_2 T^2 + p_1 T + p_0. \tag{2}$$

The polynomial coefficients $\boldsymbol{p} = (p_0, p_1, p_2)$ were obtained from the fit to the experimental data, by using the least squares method. The fits are shown by the solid curves in Fig. 4. Therefore, the bubble's volume as a function of time can be estimated from the measured LBTP signal by using calibrating coefficients $\boldsymbol{p}$.

3.3 Bubbles dynamics during the synchronized delivery of Er:YAG pulses

It is well known that the vapor bubble loses its energy during oscillations. To balance this energy dissipation, we used two Er:YAG-laser pulses delayed by 130–170 µs, as shown by the blue curves in Fig. 5. Here, the first pulse has energy of 2.0 ± 0.2 mJ, and FWHM of 0.8 ± 0.2 µs, while the energy of the second pulse was 2.2 ± 0.2 mJ and
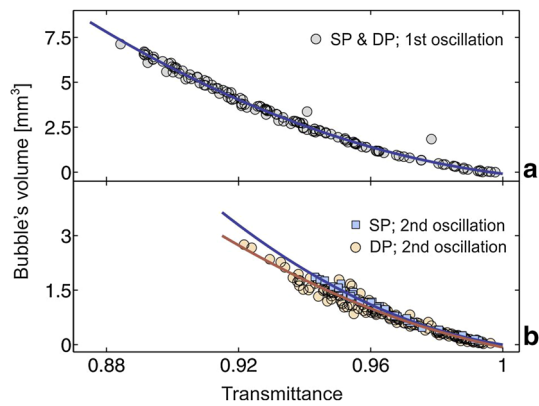
Fig. 4 Calibration of LBTP by shadow photography for the **a** first and **b** second bubbles oscillations, induced by single pulse (SP) and double pulse (DP). The calibrating points $P_i = (T_i, V_{Bi})$ are shown by *circles* and *squares*, while the *solid curves* represent the calibrating fit [Eq. (2)]
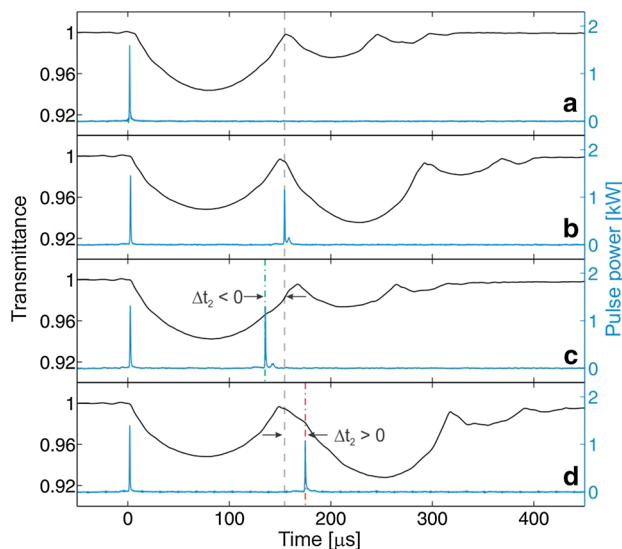

Fig. 5 Typical LBTP signals (the *left-hand-side axis* and the *black curves*) for **a** a single Er:YAG pulse and for double Er:YAG pulses, where the second pulse is delivered at **b** $\Delta t_2 = 0$, **c** $\Delta t_2 < 0$, and **d** $\Delta t_2 > 0$. The pulse powers as a function of time (the *right-hand-side axis*) are shown by the *blue curves*

its FWHM was 0.7 ± 0.2 µs. The synchronization of particular excitation pulse i can be defined by time delay Δt_i between the $(i - 1)$-th bubble's collapse and the time t_{Bi} of delivery of the i-th Er:YAG pulse (e.g., see Fig. 5c, d):

$$\Delta t_i = t_{C_{i-1}} - t_{B_i}; \quad i = 2, 3, 4, \ldots \tag{3}$$

In Eq. (3), the integer i starts with 2.

The black curve in Fig. 5a shows the LBTP signal of the bubble, induced by a single pulse. On the other hand, the black curve in Fig. 5b shows the vapor bubble's oscillations, if the second Er:YAG pulse is radiated 150 µs later

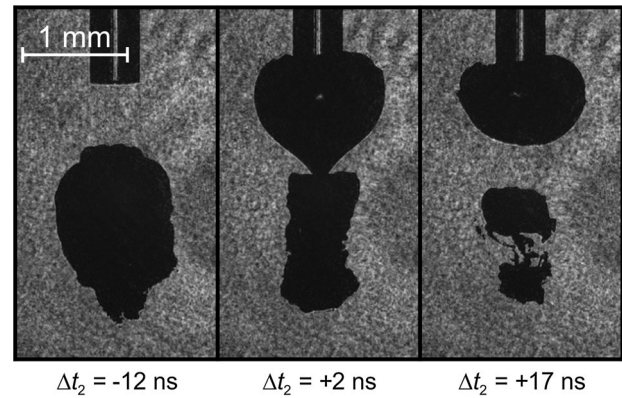Fig. 6 Shadowgraphs of a second bubble's oscillations at their maximum volumes for three different time delays Δt_2 between the first bubble's collapse and the second Er:YAG pulse

than the first one, i.e., *exactly* at the end of the first bubble's collapse ($\Delta t_2 = 0$). In this case, the synchronized delivery of additional Er:YAG energy increases the mechanical energy of the liquid medium. Consequently, the volume of the second bubble significantly increases due to the resonance effect, as is visible from the comparison of this result with the LBTP signals acquired during the single pulse (Fig. 5a). Moreover, in this case, the mechanical energy of the second oscillation is even larger than the mechanical energy of the first bubble's oscillation and the number of the oscillations increases from three (e.g., see the black curve in Fig. 5a) to four (e.g., see the black curve in Fig. 5b). This prolongs the duration of acoustic transients.

The importance of the synchronized delivery of multiple Er:YAG-laser pulses during the bubble's oscillations is clearly visible from Fig. 5c, where the black curve shows the bubble's oscillations when the second Er:YAG pulse is delivered *before* the end of the bubble's first oscillation (i.e., $\Delta t_2 < 0$). In this case, the resonance effect is not obtained and the mechanical energy of the second and the third oscillation is not increased.

Figure 5d shows the LBTP signal, when the first and the second Er:YAG pulses are delayed by 170 µs (e.g., see the blue curve). In this case, the second pulse is delivered *after* the first bubble's collapse (i.e., $\Delta t_2 > 0$). Here, we can also observe a similar effect as in the case of Fig. 5b.

From Fig. 5, it can be concluded that in the case of multiple Er:YAG pulses, it is important to not deliver the second pulse before the end of the bubble's first oscillation. Instead, the second Er:YAG-laser pulse should be delivered at the end or slightly after the bubble's collapse. In such cases, a resonance effect is obtained which increases the mechanical energy of the secondary bubble's oscillations and also prolongs their duration.

Figure 6 shows the shadowgraphs of the second bubble's oscillation when reaching its maximum volume for

three different time delays Δt_2 that are presented below each image. First image presents the second oscillation at its maximum volume, if the second pulse is delivered *before* the first bubble's collapse, i.e., at $\Delta t_2 = -12$ ns. On contrary, the other two images show the second oscillation for the case, when $\Delta t_2 > 0$. From the presented results, it is clearly visible, that only one bubble exists also during the second oscillation, if the second Er:YAG pulse is delivered *before* the first collapse, while two separate bubbles appear during the second oscillation, if the additional pulse is delivered *after* the first collapse. In the latter case, the separation increases by increasing the time delay Δt_2.

Although the result—when multiple pulses are applied in water—is quite complex, since multiple pulses can generate multiple bubbles (as visible from Fig. 6), the proposed calibration of the LBTP works quite well, as is clearly confirmed by results on Fig. 4b. This endorses the proposed and developed calibrating method as a robust and appropriate approach that enables the usage of LBTP also for measuring the bubble's volume and, consequently, its energy.

The synchronized delivery prolongs the duration of oscillating bubble. It is expected that this PHAST effect will lead to additional clinical benefits, since it is well known that when bacteria are exposed to increased destructive effects, the kill rate depends not only on the amplitude of these effects, but also—even more importantly—on their temporal duration [22]. When subjected to acoustic transients, the bacteria's structure is disrupted and the bacteria die, providing that the exposure to the transients is extensive enough to be fatal. Bacteria kill rate is thus expected to be much higher when bacteria are submitted to the synchronized delivery of multiple pulses prolonging the duration of acoustic transients. Moreover, in such a way, the bacteria can be more efficiently killed at lower amplitudes. Since higher amplitudes leads to higher collateral damage, this approach enables more efficient and safer treatment.

3.4 Oscillation energy-conversion efficiency

In our previous work [8], we defined the energy-conversion efficiency η as the ratio between the mechanical energy E_B of the bubble and the pulse energy E_L:

$$\eta = \frac{E_B}{E_L} = \frac{V_0 p_\infty}{E_L}, \tag{4}$$

where V_0 stands for the maximum volume of the first bubble oscillation and $p_\infty = 10^5$ Pa equals the hydrostatic pressure of the water. However, in the case of the synchronized delivery of multiple Er:YAG pulses, an oscillation energy-conversion efficiency should be defined. Here, the efficiency of the particular excitation pulse i can be defined as follows:

$$\eta_i = \frac{\Delta V_{0i} p_\infty}{E_{L_i}}. \tag{5}$$

In Eq. (5), E_{Li} stands for the energy of the i-th laser pulse and ΔV_{0i} is the difference of the maximum volume of the i-th oscillation with and without the i-th laser pulse. As we show by the result in Fig. 5c, the i-th pulse can also decrease the bubble's volume; therefore, oscillation efficiency, defined by Eq. (5), can take also negative values.

To estimate the efficiency, defined by Eq. (5), one has to know, what the volume of the i-th oscillation would be, if the i-th pulse will not be delivered. For example, for double-pulse regime, we can measure the volume of the second bubble's oscillation from the LBTP signal, by using calibrating coefficients obtained from Eq. (2). However, we need to know, what the volume of the second oscillation would be, if only a single pulse would be used. We will show that this is possible to calculate from the volume of the first oscillation.

By using LBTP, we measured the volumes V_{01} of the first oscillation and volumes V_{02} of the second oscillations induced by a single pulse. The measured data are shown by dots in Fig. 7. From Fig. 7, it can be seen that V_{02} linearly depends on V_{01}. Therefore, the coefficient $\gamma_{i \to i+1}$ can be obtained by linear fit to the experimental data:

$$V_{0_{i+1}} = \gamma_{i \to i+1} V_{0_i}. \tag{6}$$

By using Eqs. (5) and (6), the oscillation energy-conversion efficiency can be calculated from the measured data as follows:

$$\eta_i = \frac{p_\infty (V_{0_i} - \gamma_{i \to i+1} V_{0_{i-1}})}{E_{L_i}}. \tag{7}$$

In such a way, we measured the oscillation energy-conversion efficiency of the second oscillation induced by double pulse as a function of time delay Δt_2 (see Eq. (3) for $i = 2$). The results are shown by circles in Fig. 8. For
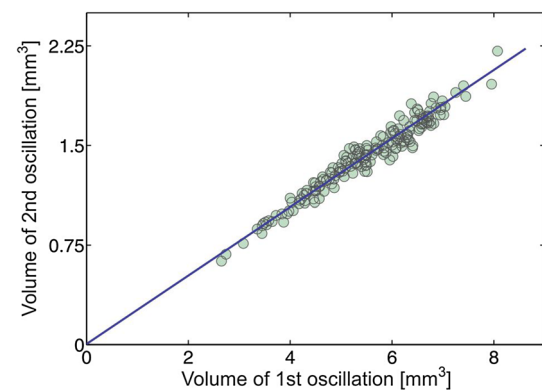

Fig. 7 Maximum volume of the second oscillation as a function of the maximum volume of the first oscillation, induced by a single pulse. The measured data are shown by *dots*, while the *solid line* represents the fit of Eq. (6)
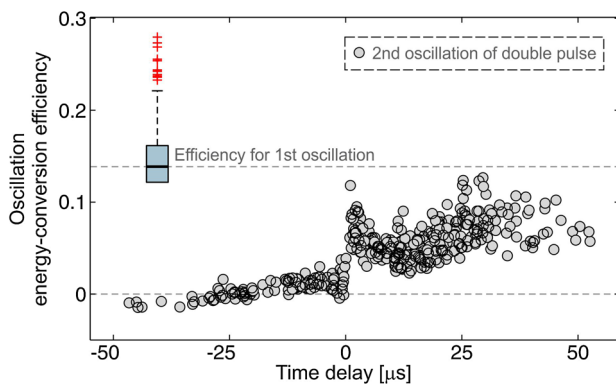
Fig. 8 The oscillation energy-conversion efficiency of the second oscillation (η_2) induced by double pulse as a function of time delay Δt_2. For the comparison, the energy-conversion efficiency for the first oscillation is shown by a *box* plot

comparison, the box plot (inserted in Fig. 8) shows the energy-conversion efficiency for the first oscillation.

From the measured data in Fig. 8, we can see that efficiency η_2 reaches negative values for time delays $\Delta t_2 < -25$ µs. This happens since at these delays, and the second pulse retards the second bubble's oscillation. On the other hand, a resonance effect is obtained at delays slightly larger than $\Delta t_2 = 0$. This resonance firstly decreases with increasing delay and then starts approaching the values for the energy-conversion efficiency of the first oscillation with increasing Δt_2. This limit can be explained by the fact that in a limit $\Delta t_2 \to \infty$, double-pulse regime becomes equivalent to the single-pulse regime.

4 Conclusions

By using a laser beam transmission probe, we studied the synchronized delivery of Er:YAG-laser pulses into water that has the potential to enhance the endodontic treatment. To overcome the main drawbacks of the LBTP method, we proposed a calibration by simultaneous employment of the shadow photography. The proposed calibration proved as robust and appropriate also in cases when multiple pulses induce two separated bubbles. The same approach can be therefore also applied in other experiments where LBTP represents a useful tool for examination of laser-induced bubble's in liquids.

We have shown that in case of the delivery of multiple laser pulses, the resonance effect is obtained when the second pulse is delivered at the end or slightly after the bubble's first collapse. In this case, the resonance effect increases the mechanical energy of the secondary oscillations. On the other hand, if the second pulse is delivered before the end of the bubble's first oscillation, it decreases the oscillation energy-conversion efficiency as well as it decreases the duration of bubble's oscillations and, therefore, decreases the efficiency of the laser treatment.

References

1. M. Lukač, G. Pustovrh, J. LA&HA **2013**, 1 (2013)
2. E. DiVito, O.A. Peters, G. Olivi, Lasers. Med. Sci. **27**, 273 (2012)
3. E. Deleu, M. Meire, R.G. Moor, Lasers. Med. Sci. **30**, 831 (2015)
4. G.M. Hale, M.R. Querry, Appl. Opt. **12**, 555 (1973)
5. M. Mrochen, P. Riedel, C. Donitzky, T. Seiler, J. Biomed. Opt. **6**, 344 (2001)
6. A. Vogel, V. Venugopalan, Chem. Rev. **103**, 577 (2003)
7. K. Iwai, Y.W. Shi, K. Nito, Y. Matsuura, T. Kasai, M. Miyagi, S. Saito, Y. Arai, N. Ioritani, Y. Okagami, M. Nemec, J. Sulc, H. Jelinkova, M. Zavoral, O. Kohler, P. Drlik, Appl. Opt. **42**, 2431 (2003)
8. P. Gregorčič, M. Jezeršek, J. Možina, J. Biomed. Opt. **17**, 075006 (2012)
9. W. Lauterborn, T. Kurz, Rep. Prog. Phys. **73**, 106501 (2010)
10. R. Petkovšek, P. Gregorčič, J. Appl. Phys. **102**, 044909 (2007)
11. P. Gregorčič, M. Jamšek, M. Lukač, M. Jezeršek, J. LA&HA **2014**, 14 (2014)
12. R. Tanabe, T.T.P. Nguyen, T. Sugiura, Y. Ito, Appl. Surf. Sci. **351**, 351 (2015)
13. L.F. Devia-Cruz, F.G. Perez-Gutierrez, D. Garcia-Casillas, G. Aguilar, S. Camacho-Lopez, D. Banks, Atom. Sprays **23**, 475 (2013)
14. A. Matsumoto, A. Tamura, A. Kawasaki, T. Honda, P. Gregorčič, N. Nishi, K. Amano, K. Fukami, T. Sakka, Appl. Phys. A **122**(234), 1–6 (2016)
15. R. Petkovšek, P. Gregorčič, J. Appl. Phys. **102**, 044909 (2007)
16. P. Gregorčič, R. Petkovšek, J. Možina, J. Appl. Phys. **102**, 094904 (2007)
17. T. Sakka, A. Tamura, A. Matsumoto, K. Fukami, N. Nishi, B. Thornton, Spectrochim. Acta Part B **97**, 94 (2014)
18. K. Sasaki, T. Nakano, W. Soliman, N. Takada, Appl. Phys. Express **2**, 046501 (2009)
19. G.S. Settles, *Schlieren and Shadowgraph Techniques* (Springer, Berlin, 2001)
20. P. Gregorčič, R. Petkovšek, J. Možina, G. Močnik, Appl. Phys. A **93**, 901 (2008)
21. E.D. Jansen, T. Asshauer, M. Frenz, M. Motamedi, G. Delacretaz, A.J. Welch, Laser Surg. Med. **18**, 278 (1996)
22. D.M. Simanovskii, M.A. Mackanos, A.R. Irani, C.E. O'Connell-Rodwell, C.H. Contag, H.A. Schwettman, D.V. Palanker, Phys. Rev. E **74**, 011915 (2006)